Modeling diffusion in discontinuous media under generalized discontinuous interface conditions, Part II: application to conductive heat transport

Elisa Baioni, Antoine Lejay, Géraldine Pichot, Giovanni Michele Porta

Modeling diffusion in discontinuous media under generalized discontinuous interface conditions, Part II: application to conductive heat transport

Elisa Baioni[1], Antoine Lejay[2], Géraldine Pichot[3], and Giovanni Michele Porta[1]

[1]Politecnico di Milano, Department of Civil and Environmental Engineering, 20133 Milan (IT)
[2]Université de Lorraine, CNRS, Inria, IECL, F-54000 Nancy, France; ORCID: 0000-0003-0406-9550
[3]Inria - 2 rue Simone Iff, 75589 Paris, France and Université Paris-Est, CERMICS (ENPC), 6 et 8 av. Blaise Pascal, 77455 Marne-la-Vallée Cedex 2, France

Abstract

We consider heat transport within a discontinuous domain by relying on the modeling approach proposed by Baioni et al. in part I of this paper. Such approach has been specifically designed to address diffusive processes in media with discontinuous physical properties and generalized boundary conditions at the discontinuities. Three algorithms are here applied to estimate the conductive heat transport in a bimaterial medium. The algorithms undergo testing using two test cases that share the same computational domain but differ in terms of their initial conditions. According to the numerical results all the algorithms ensure the conservation of thermal energy and preserve thermal equilibrium under steady state conditions. The Generalized Uffink Method (GUM) and Generalized HYMLA (GHYMLA) demonstrate sensitivity to the choice of the time step, whereas the Generalized Skew Brownian Motion (GSBM) appears to be unaffected by the value of Δt. The GUM algorithm presents an optimal trade-off between accuracy and computational time.

Keywords– Discountinuous media, thermal diffusivity, conductive heat transport, numerical simulation, random walk methods

1 Introduction

Discontinuous media, characterized by irregular interfaces and varying material properties, are encountered in a wide range of systems, including porous materials, composite structures, and multiphase systems. Heat transfer across different media is a phenomenon that affects numerous environmental [19, 24] and engineering processes [12, 7, 4, 18, 28] and stands as a vital component of clean and sustainable energy systems. For example, porous media play a crucial role in heat exchange within electronic cooling, heat exchangers, and various thermal systems. As discussed in various studies [11, 22, 21], the existence of abrupt changes in material properties and/or physical conditions within a medium can introduce significant challenges when modeling heat transfer phenomena.

Conductive heat transfer in layered composite materials has been widely addressed in the literature, where analytical solutions have been presented [5, 1] for simple geometries and a prescribed set of initial and boundary conditions. To overcome these limiting assumptions numerous literature works deal with numerical simulation tools. Numerical analysis of heat transfer processes can be performed by direct numerical simulation based on computational fluid dynamics tools (e.g., [18]), these methods being limited to small size samples due to computational constraints. Alternative approaches are based on probabilistic simulations based on Monte Carlo approaches [9, 6, 27, 23], or on pore network modeling [14, 13, 15], that allow analyzing larger systems by conceptualizing the geometry through a interconnected network of simplified pores and throats.

This study addresses heat transport in a discontinuous medium relying on the random walk approaches introduced in [2]. These latter enable the resolution of diffusive processes in domains characterized by discontinuous physical properties and generalized interface conditions. Random walk particle tracking approaches have been widely employed to simulate advective-diffusive mass transfer in porous domains. In this context these class of Lagrangian methods have proven useful as simulation methods and have facilitated the development of conceptual and mathematical models to upscale pore-scale properties [20, 25]. For diffusive mass transfer several algorithms can be applied to deal with the presence of spatially discontinuous diffusion coefficients [17]. Yet, the same methodologies cannot be applied to heat transfer, because of the inherent difference in the problem parameterization between heat and mass transfer. Notably, the coefficient driving heat transfer by conduction within a material (often called thermal diffusivity) is different than the conductivity coefficient, which is conversely applied to guarantee heat flux continuity across an interface. The applicability of classical random walk methods to heat transfer processes is thus strictly limited to homogeneous media. In part I of this paper a general theory and solution algorithms are developed to deal with generalized interface conditions across an interface [2]. In this paper we explicitly show how

such theory can be leveraged to simulate conductive heat transport across materials characterized by discontinuous properties. To overcome the above mentioned limitations of existing methods in approximating Fourier's law, which governs heat transport, we have proposed a new formulation through a convenient transformation implementing a Lagrangian method with a weight associated to each particle. Ultimately the developed approaches provide a critical extension of available Lagrangian methods and pave the way towards the application of such methods to a new class of problems. We employ two test cases dealing with heat transfer in a bimaterial domain and benchmarked against an analytical solution. Two test cases, each involving the same computational domain but different initial conditions, are presented to evaluate the performance of the algorithms in estimating heat transport in discontinuous media.

The paper is structured as: Section 2 presents the application of the three generalized interface algorithms, i.e. the generalized Uffink, HYMLA and Skew Brownian Motion algorithms, here labeled as GUM, GHYMLA and GSBM respectively. The benchmark tests used to evaluate the algorithms' performance are described in Section 3, as well as a discussion of the numerical results. The conclusions drawn from our study are reported in Section 4.

2 Heat transport in a bimaterial medium

We start from the approach implemented in part I of this paper [2] to solve diffusive transport in discontinuous media under generalized conditions at the discontinuity interface. Here we consider one-dimensional thermal diffusion process through a random walk. The GUM, GHYMLA and GSBM algorithms reported in the Supplementary Material are used to assess conductive heat transfer in a bimaterial medium, as in Figure 1, with a piece-wise constant diffusivity D discontinuous at $X_I = 0$. The discontinuity interface is perceived as a semi-reflective barrier and divides the domain in R_1 for $x < 0$ and R_2 for $x > 0$ with a diffusivity equal to D_1 and D_2, respectively. The theoretical formulation of the physical problem and the derivation of the model constants for the case study are illustrated in the following.

2.1 Properties of heat transport

The GUM, GSBM and GHYMLA algorithms discussed in [2], solve diffusive problems in discontinuous media with generalized boundary conditions at the discontinuity interface.

We now present how to apply these methods to a heat transport problem. Actually, this kind of problem cannot be treated directly by applying GUM, GSBM or GHYMLA so that we introduce a convenient transform. More precisely, we consider solving the Fourier's law [8]

with an interface at 0 and an initial condition ψ:

$$\phi(y)\partial_t T(t,y;\psi) = \mathcal{F}_y T(t,y;\psi), \tag{1}$$
$$T(t,0^-;\psi) = T(t,0^+;\psi), \tag{2}$$
$$k_1 \nabla T(t,0^-;\psi) = k_2 \nabla T(t,0^+;\psi), \tag{3}$$
$$T(0,y;\psi) = \psi(y), \tag{4}$$

where $T(t,y;\psi)$ is the temperature at time t and point y,

$$\mathcal{F}_y f(y) := \nabla_y(k(y)\nabla_y f(y)) \text{ and } \phi(y) := \rho(y)c(y).$$

Here, ρ, c and k are functions constant on each side of the interface located at 0. For such functions f, we write $f(y) = f_1$ if $y < 0$ and f_2 if $y > 0$. The constants are the *thermal conductivity* k_i [$\mathrm{W\,m^{-1}\,K^{-1}}$], the *specific heat* c_i [$\mathrm{J\,kg^{-1}\,K^{-1}}$], and the *density* ρ_i [$\mathrm{kg\,m^{-3}}$]. All these constants are assumed to be positive.

First, we consider the problem in free space, and later in a finite domain $[-L, L]$ with reflected boundary conditions at each side. The computations are the same in such a case.

Integrating (1) on the domain and using the Green formula,

$$\begin{aligned}\partial_t \int_{-\infty}^{+\infty} \phi(y)T(t,y;\psi)\,\mathrm{d}y &= \int_{-\infty}^{0} \nabla_y(k(y)\nabla_y T(t,y;\psi))\,\mathrm{d}y + \int_{0}^{+\infty} \nabla_y(k(y)\nabla_y T(t,y;\psi))\,\mathrm{d}y \\ &= k_1 \nabla T(t,0-;\psi) - k_2 \nabla T(t,0+;\psi) = 0. \end{aligned} \tag{5}$$

Hence, the quantity $\int_{-\infty}^{+\infty} \phi(y)T(t,y;\psi)\,\mathrm{d}y$ is conserved over time. On the other hand we observe that,

$$\begin{aligned}\partial_t \int_{-\infty}^{+\infty} T(t,y;\psi)\,\mathrm{d}y &= \int_{-\infty}^{0} \frac{1}{\phi_1}\nabla_y(k_1 \nabla_y T(t,y;\psi))\,\mathrm{d}y + \int_{0}^{+\infty} \frac{1}{\phi_2}\nabla_y(k_2 \nabla_y T(t,y;\psi))\,\mathrm{d}y \\ &= \frac{k_1}{\phi_1}\nabla T(t,0-;\psi) - \frac{k_2}{\phi_2}\nabla T(t,0+;\psi). \end{aligned} \tag{6}$$

Therefore, the quantity $\int_{-\infty}^{+\infty} T(t,y;\psi)\,\mathrm{d}y$ is *not* conserved over time.

2.2 Lagrangian approach

As practical implication of (5) we design a numerical scheme relying upon a Lagrangian approach where the thermal energy of the system is discretized by a set of particles, each one carrying a specific quantity. The design of such diffusive Lagrangian scheme is achieved by defining a fundamental solution $q(t,x,y)$ [$\mathrm{m^{-1}}$] such that $q(t,x,y)\,\mathrm{d}y$ is the probability that

a particle starting from x ends in a small volume $\mathrm{d}y$ around y at time t. We relate q and T through

$$T(t, y; \psi) = \int \psi(x) q(t, x, y) \frac{\phi(x)}{\phi(y)} \, \mathrm{d}x. \tag{7}$$

Here, q is the family of solutions to

$$\partial_t q(t, x, y) = \mathcal{L}_y q(t, x, y), \tag{8}$$

$$\frac{1}{\phi_1} q(t, x, 0^-) = \frac{1}{\phi_2} q(t, x, 0^+), \tag{9}$$

$$\alpha_1 \nabla q(t, x, 0-) = \alpha_2 \nabla q(t, x, 0+), \tag{10}$$

$$\lim_{t \to 0} q(t, x, y) = \delta_x(y), \tag{11}$$

where

$$\mathcal{L}_y f(y) = \nabla_y (\alpha(y) \nabla_y f(y)) \text{ with } \alpha_i := \frac{k_i}{\rho_i c_i} \, [\mathrm{W\,m^2\,J^{-1}}], \ i = 1, 2,$$

for any suitable function f. The quantity α is the *thermal diffusivity*.

With (11) and (7), we obtain that $\lim_{t \to 0} T(t, y; \psi) = \psi(y)$. With (9) and (10), $T(t, \cdot; \psi)$ satisfies the interface conditions (2) and (3). We note that (8)-(11) is formulated as a diffusive process in a discontinuous medium with generalized interface conditions, as indicated in Section 2 of [2], by assuming

$$D_i = \alpha_i, \ \nu_i = \frac{1}{\phi_i} = \frac{1}{\rho_i \, c_i} \text{ and } \kappa_i = \alpha_i \text{ for } i = 1, 2.$$

Hence, a closed-form expression for q is given by the method of images. The mass conservation property (12) holds.

$$\beta^2 = \frac{D_2}{D_1} = \frac{1 + \gamma}{1 - \gamma} = \frac{\kappa_2}{\kappa_1}. \tag{12}$$

We also note that $q(t, x, y)$ is positive for any $t > 0$ and any $x, y \in \mathbb{R}$ and satisfies both the Kolmogorov backward equation in (13) and the *Chapman-Kolmogorov equation*.

$$\partial_t q(t, x, y) = \nabla_x (\alpha(x) \nabla_x q(t, x, y)) \tag{13}$$

with the interface conditions

$$q(t, 0-, y) = q(t, 0+, y) \text{ and } k_1 \nabla_x q(t, 0-, y) = k_2 \nabla_x q(t, 0+, y) \text{ for any } y.$$

From the properties of the fundamental solution, $q(t,x,y)$ satisfies

$$q(t+s,x,y) = \int_{\mathbb{R}} q(s,x,z)q(t,z,y)\,\mathrm{d}z \text{ for any } s,t>0,\ x,y\in\mathbb{R}. \tag{14}$$

The positivity and the mass conservation are sufficient to interpret $q(t,x,\cdot)$ as a probability density. The Chapman-Kolmogorov property ensures that moving the particle again on time steps t and s is the same as performing one step at time $s+t$ (the so-called *Markov property*).

Finally, since $\mathcal{L}_y\phi(y)=0$, it follows from (13) that

$$\partial_t \int \phi(x)q(t,x,y)\,\mathrm{d}x = \int \phi(x)\nabla_x(\alpha(x)\nabla_x q(t,x,y))\,\mathrm{d}x$$

and using the Green formula twice,

$$\partial_t \int \phi(x)q(t,x,y)\,\mathrm{d}x = 0.$$

Hence, ϕ is an invariant measure for q. It corresponds to the *steady state*. With (7), $t\mapsto T(t,y;1)$ is constant.

2.2.1 Setting up the Lagrangian method

To solve the one-dimensional thermal diffusion process, we design a Lagrangian method based on N particles and applied to a finite domain $[-L,L]$ with reflection boundary conditions. As mentioned in [2], when we are restricted to the finite domain, the closed-form expression q has to be replaced by a fundamental solution q_L that still satisfies both the Kolmogorov forward equation and the Kolmogorov backward equation with the additional conditions

$$\nabla_x q_L(t,\pm L,y) = \nabla_y q_L(t,x,\pm L) = 0.$$

At the boundaries $\pm L$, $q(t,x,\cdot)$ approximates q_L when $|x|^2/t \ll 1$ (for an interface at 0) and $t\ll 1$. The methods GUM, GSBM and GHYMLA allows one to sample particles' position according to the density. The constants required by the computational algorithms are provided in Table (1), as a function of the physical properties of the involved materials.

For each particle the position $X(0)$ is drawn from a prescribed given initial distribution ν over $[-L,L]$, in line with the considered initial condition. At any time t the position $X(t)$ is determined according to the transition probability density $q_L(t,X(0),\cdot)$. For this, thanks to the Chapman-Kolmogorov equation, we fix a time step $\Delta t = t/n$ and we draw iteratively $X((k+1)\Delta t)$ from any suitable approximation of $q_L(t,X(k\Delta t),\cdot)$. Thus, $\{X(k\Delta t)\}_{k=0,\dots,n}$

Table 1: Constants in the algorithms for the Fourier's law with interface.

Algorithm	Parameters
GUM	$A = \frac{\rho_1 c_1\sqrt{\alpha_1}-\rho_2 c_2\sqrt{\alpha_2}}{\rho_1 c_1\sqrt{\alpha_1}+\rho_2 c_2\sqrt{\alpha_2}}$ $\quad B = \frac{2\rho_2 c_2\sqrt{\alpha_2}}{\rho_1 c_1\sqrt{\alpha_1}+\rho_2 c_2\sqrt{\alpha_2}}$ $\widetilde{A} = \frac{\rho_2 c_2\sqrt{\alpha_2}-\rho_1 c_1\sqrt{\alpha_1}}{\rho_1 c_1\sqrt{\alpha_1}+\rho_2 c_2\sqrt{\alpha_2}}$ $\quad \widetilde{B} = \frac{2\rho_1 c_1\sqrt{\alpha_1}}{\rho_1 c_1\sqrt{\alpha_1}+\rho_2 c_2\sqrt{\alpha_2}}$
GSBM, GHYMLA	$\theta_g = \frac{\rho_2 c_2\sqrt{\alpha}_2-\rho_1 c_1\sqrt{\alpha}_1}{\rho_2 c_2\sqrt{\alpha}_2+\rho_1 c_1\sqrt{\alpha}_1}$

performs a random walk, and the distribution of $X(t)$ is close to $q_L(t, X(0), \cdot)$. The particle's behavior is determined according to the region of the domain where the particle lies at each time step:

1. $X(t) \in I = [-\sqrt{6D_1\Delta t}, \sqrt{6D_2\Delta t}]$: the particle resides in the *interface layer* containing the interface point $X_I = 0$. The position $X(t+1)$ is sampled from $q(\Delta t, x, \cdot)$, or any of its approximations.

2. $X(t) \in B_{-L} = [-L, -L + \sqrt{6D_1\Delta t}]$ or $X(t) \in B_L = [L - \sqrt{6D_2\Delta t}, L]$: the particle belongs to the *boundary layer*. The next particle's position is sampled from a Gaussian step (GSBM) or a uniform step (GUM or GHYMLA). The particle is reflected when it reaches the boundary $x = \pm L$.

3. $X(t) \notin (I \cup B_{\pm L})$: $X(t+1)$ is determined by performing an usual step using a Gaussian (GSBM) and or a uniform (GUM or GHYMLA) step.

The size of the interfaces and boundary layers are function of Δt, the latter being selected so that $I \cap B_L = I \cap B_{-L} = \emptyset$.

Physical quantities of the domain can be recovered by properly counting the particles. We are given an initial profile ψ which is an integrable, non-negative function on $[-L, L]$. For the k-th particle among the N particles, we draw the initial position $X^{(k)}(0)$ of a particle according to the initial distribution $x \mapsto \phi(x)\psi(x)/E$ with $E := \int_{-L}^{L} \psi(x)\phi(x)\,\mathrm{d}x$. The particle is then moved to $X^{(k)}(t)$ using one of scheme described above.

We associate with the k-th particle the "weight" $w_k := EN^{-1}\phi(X^{(k)}(t))^{-1}$.

Given $g : [-L, L] \to \mathbb{R}$, the *mean operator* is

$$\mathcal{M}(g; t, N, \psi) := \sum_{k=1}^{N} w_k\, g(X^{(k)}(t)) = \frac{E}{N}\sum_{k=1}^{N} \frac{g(X^{(k)}(t))}{\phi(X^{(k)}(t))}.$$

According to the strong law of large numbers (and assuming that we use an exact scheme),

$$\begin{aligned}\lim_{N\to\infty} \mathcal{M}(g;t,N,\psi) &= E\int_{-L}^{L}\int_{-L}^{L} \frac{\phi(x)\psi(x)}{E} q_L(t,x,y)\frac{g(y)}{\phi(y)}\,\mathrm{d}y\,\mathrm{d}x \\ &= \int_{-L}^{L}\int_{-L}^{L} \psi(x) q_L(t,x,y)\frac{\phi(x)}{\phi(y)} g(y)\,\mathrm{d}y\,\mathrm{d}x \\ &= \int_{-L}^{L} T(t,y;\psi) g(y)\,\mathrm{d}y.\end{aligned} \tag{15}$$

For counting the particles around a given point, we decompose the domain $[-L, L]$ into N_a non-overlapping cells $A_i := [x_{i-1}, x_i]$ for $i = 1, \ldots, N_a$ where the interface $0 = x_i$ for some index i, $x_0 = -L$, $x_{N_a} = L$. We write $a_i := (x_{i-1} + x_i)/2$, the midpoint of the cell A_i, and $|A_i| := x_i - x_{i-1}$, the length of the cell A_i.

We take $g_i(y) := \frac{1}{|A_i|}\mathbb{1}_{A_i}(y)$. Then

$$\mathcal{M}(g_i;t,N,\psi) \approx \frac{1}{|A_i|}\frac{E}{\phi(a_i)}\frac{n(t,A_i)}{N} \tag{16}$$

with

$$n(t,A) := \sum_{i=1}^{N} \mathbb{1}_A(X^{(k)}(t)) \tag{17}$$

3 Benchmark tests

Heat transfer in a one-dimensional bimaterial medium of finite size $[-L, L]$ with reflecting boundary conditions (RBC) as displayed in Figure 1 is simulated by the GUM Algorithm (Algorithm 1 in Supplementary Material), GSBM Algorithm (Algorithm 2 in Supplementary Material) and GHYMLA Algorithm (Algorithm 3 in Supplementary Material). The domain consists of two regions divided by an interface $X_I = 0$, *i.e.*, R_1 for $x < 0$ and R_2 for $x > 0$. The physical properties, such as density (ρ), thermal conductivity (k), specific heat (c), and thermal diffusivity (α), are constant within R_1 and R_2. The algorithms are tested by considering two case studies:

- **Case 1: Thermal equilibrium**
  Domain: The two layers are initialized in thermal equilibrium, *i.e.*, (20)-(21) holds.
  Aim: Check the conservation of the equilibrium temperature of each layer and the thermal energy.

- **Case 2: Thermal gradient**
  Domain: An initial temperature difference is applied only on the region R_2.

Aim: Check that the temperature distribution along the domain is consistent with the analytical solution (23) over time.

All benchmark tests have the same domain size and physical properties as those described in Table 2, but their initial conditions differ. Each test assumes the domain boundaries at $x = \pm L$ are reflective barriers (*i.e.*, no-flux boundary conditions).

For each simulation, the average computational time t_{cm} [s] is computed as the time to complete the entire simulation divided by the number of steps. Each simulation is performed in Matlab with an Intel(R) Xeon(R) CPU E5-2640 v3 @ 2.60GHz processor. The computational parameters are indicated in Table 3.

Table 2: Size and physical properties of the domain used in the tests.

	R_1	R_2	parameter	SI units
k	0.603	0.335	thermal conductivity	$\mathrm{W\,m^{-1}\,K^{-1}}$
ρ	1000	1600	density	$\mathrm{kg\,m^{-3}}$
c	4184	753	specific heat	$\mathrm{J\,kg^{-1}\,K^{-1}}$
L	0.005	0.005	length of the domain region	m
X_I	0		position of the interface	m

Table 3: Case 1: Computational and schemes parameters for simulation

N_p	Δt			
2×10^6	0.01			
θ_g	A	B	$\widetilde{A}$	$\widetilde{B}$
-0.4286	0.4286	0.5714	-0.4286	1.4286

3.1 Case 1: Thermal equilibrium

The test is performed to verify that the GUM, GSBM and GHYMLA algorithms maintain the temperature within each layer constant over time under steady-state equilibrium condition. Here we provide the theoretical benchmark results to assess the Lagrangian formulations outlined in 2.2 followed by the numerical results.

3.1.1 Theoretical benchmark solution

We deduce from the Kolmogorov backward equation presented in [2] that

$$\partial_t T(t,y;\psi) = \partial_t \int_{-L}^{L} \psi(x) q_L(t,x,y) \frac{\phi(x)}{\phi(y)} \,\mathrm{d}x = \int_{-L}^{L} \psi(x) \frac{\phi(x)}{\phi(y)} \nabla_x (\alpha(x) \nabla_x q_L(t,x,y)) \,\mathrm{d}x.$$

Assume that $\psi(x) = \psi_1$ if $x < 0$ and $\psi(x) = \psi_2$ if $x > 0$. From the Green formula,

$$\begin{aligned}
&\int_{-L}^{L} \psi(x) \frac{\phi(x)}{\phi(y)} \nabla_x (\alpha(x) \nabla_x q_L(t,x,y)) \,\mathrm{d}x \\
&= \int_{-L}^{0} \psi(x) \frac{\phi(x)}{\phi(y)} \nabla_x (\alpha(x) \nabla_x q_L(t,x,y)) \,\mathrm{d}x + \int_{0}^{L} \psi(x) \frac{\phi(x)}{\phi(y)} \nabla_x (\alpha(x) \nabla_x q_L(t,x,y)) \,\mathrm{d}x \\
&= \frac{1}{\phi(y)} \left(\psi_1 \phi_1 \alpha_1 \nabla_x q_L(t,0-,y) - \psi_2 \phi_2 \alpha_2 \nabla_x q_L(t,0+,y) \right), \quad (18)
\end{aligned}$$

since $\nabla_x q_L(t,\pm L,y) = 0$ as we use the reflected boundary conditions. Owing to the interface conditions of the Kolmogorov backward equation,

$$\begin{aligned}
\partial_t T(t,y;\psi) &= \frac{1}{\phi(y)} \left(\psi_1 \phi_1 \alpha_1 \nabla_x q_L(t,0-,y) - \psi_2 \phi_2 \alpha_2 \nabla_x q_L(t,0+,y) \right) \\
&= \frac{1}{\phi(y)} (\psi_1 - \psi_2) k_2 \nabla_x q_L(t,0+,y).
\end{aligned}$$

We then obtain that

$$T(t,y;\psi) = \psi(y) + (\psi_1 - \psi_2) \frac{k_2}{\phi(y)} \int_0^t \nabla_x q_L(s,0+,y) \,\mathrm{d}s. \quad (19)$$

When ψ equal to a constant T_0, $T(t,y;T_0) = T_0$ for any y, being also an immediate consequence from (19). This implies that

$$\int_{-L}^{0} T(t,y;T_0) \,\mathrm{d}y = \int_{-L}^{0} T(0,y;T_0) \,\mathrm{d}y = LT_0, \quad (20)$$

$$\int_{L}^{1} T(t,y;T_0) \,\mathrm{d}y = \int_{0}^{L} T(0,y;T_0) \,\mathrm{d}y = LT_0. \quad (21)$$

Using the notation (17) with $R_1 = [-L,0]$ and $R_2 = [0,L]$, we estimate these quantities by

$$\begin{aligned}
\int_{0}^{L} T(t,y;T_0) \,\mathrm{d}y &\approx \mathcal{M}(\mathbb{1}_{[0,L]};t,N,T_0) = T_0 L \frac{\phi_1 + \phi_2}{\phi_2} \frac{n(t,R_2)}{N}, \\
\int_{-L}^{0} T(t,y;T_0) \,\mathrm{d}y &\approx \mathcal{M}(\mathbb{1}_{[-L,0]};t,N,T_0) = T_0 L \frac{\phi_1 + \phi_2}{\phi_1} \frac{n(t,R_1)}{N}
\end{aligned}$$

when $X(0)$ is distributed using the measure $\phi(x)/\int_{-L}^{L}\phi(x)\,\mathrm{d}x$. Since ϕ is piecewise constant, the distributions of $X(0)$ given $X(0)<0$ is uniform over $[-L,0]$ and the distribution of $X(0)$ given $X(0)>0$ is uniform over $[0,L]$. Besides,

$$\mathbb{P}[X(0)\in R_i]=\frac{\phi_i}{\phi_1+\phi_2}\approx\frac{n(0,R_i)}{N}\text{ for }i=1,2.$$

Therefore,

$$\frac{n(0,R_1)}{n(0,R_2)}\approx\frac{\phi_1}{\phi_2}=\frac{\rho_1 c_1}{\rho_2 c_2}.$$

To check (20)-(21), it is sufficient to check that

$$\frac{n(t,R_1)}{n(0,R_1)}\approx 1\text{ and }\frac{n(t,R_2)}{n(0,R_2)}\approx 1\text{ for any }t\geq 0. \tag{22}$$

3.1.2 Numerical results

The population of N particles is split in two sub-populations with respective sizes N_1 and N_2 such that $N_1+N_2=N$ and $N_1/N_2=\rho_1c_1/\rho_2c_2$. The particles from the first sub-population are uniformly distributed on $[-L,0]$, the ones of the second sub-population are uniformly distributed on $[0,L]$, as displayed in Figure 1. We then check the conservation of the thermal equilibrium by using (22).

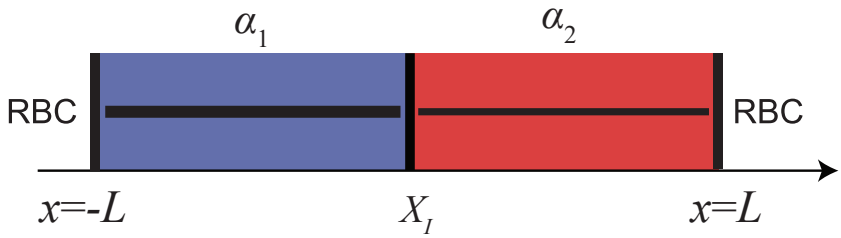

Figure 1: Case 1 setup: blue and red-filled regions indicate R_1, R_2, the continuous black lines indicate initial uniform particle placement in the two layers, different line thickness is used to indicate different particle density.

In our numerical test we set $N_1=2\times10^6$ and $N_2=5.759\times10^5$. For all algorithms, simulations are run until $t=1\,\mathrm{s}$ with the same time step equal to $10^{-2}\,\mathrm{s}$ to facilitate comparison.

The standard deviation σ of the ratio $n(t,R_i)/N_i$ is used as indicator to evaluate the performance of the algorithm, lowest values of σ indicating better performance. Results in Table 4 indicate that the three algorithms provide a standard deviation of the same order of magnitude with the highest value observed in the GHYMLA. We observe no significant trends in the results reported in Figure 2 thus we conclude that the GUM, GSBM and GHYMLA algo-

rithms guarantee thermal energy conservation and maintain the temperature constant under steady-state equilibrium conditions.

Table 4: Case 1: Standard deviation σ of $n(t, R_i)/N_i$ for the GUM, GSBM and GHYMLA algorithm.

	GUM	GSBM	GHYMLA
σ	2.342×10^{-4}	2.316×10^{-4}	2.681×10^{-4}

3.2 Case 2: Thermal gradient

The test case simulates heat transport and the local temperature evolution in a bimaterial medium subjected to an initial temperature difference (see Figure 3) using the GUM, GSBM and GHYMLA algorithms. The numerical results are presented here after a theoretical formulation of the physical problem.

3.2.1 Theoretical benchmark solution

We follow the approach specified below. Set $\psi(x) = T_0 \mathbb{1}_{[0,L]}(x)$, that is the Heaviside function, so that $\psi_1 = 0$, $\psi_2 = T_0$ for T_0 a temperature in K. Replacing q_L by q in (19),

$$T(t, y; T_0 \mathbb{1}_{[0,L]}) = T_0 \mathbb{1}_{[0,L]}(y) - \frac{k_2}{\phi(y)} T_0 \int_0^t \nabla_x q_L(s, 0+, y)\, \mathrm{d}s.$$

Replacing $q_L(s, 0+, y)$ by $q(s, 0+, y)$ and using the closed-form of the density transition function q in [2] we obtain

$$T(t, y; T_0 \mathbb{1}_{[0,L]}) \approx T_0 \frac{\sqrt{k_2 \rho_2 c_2}}{\sqrt{k_2 \rho_2 c_2} + \sqrt{k_1 \rho_1 c_1}} \times \begin{cases} \operatorname{erfc}\left(\dfrac{|y|}{2\sqrt{\alpha_1 t}}\right) & \text{for } y < 0, \\ 1 + \dfrac{\sqrt{k_1 \rho_1 c_1}}{\sqrt{k_2 \rho_2 c_2}} \operatorname{erf}\left(\dfrac{y}{2\sqrt{\alpha_2 t}}\right) & \text{for } y > 0. \end{cases} \tag{23}$$

Such an expression is already found in [3].

On the other hand, using the notations of Section 2.2.1,

$$\begin{aligned} T(t, a_i; T_0 \mathbb{1}_{[0,T]}) &\approx \int_{-L}^{L} T(t, y; T_0 \mathbb{1}_{[0,L]}) g_i(y)\, \mathrm{d}y \\ &\approx \mathcal{M}(g_i; t, N, T_0 \mathbb{1}_{[0,L]}) = T_0 \frac{L}{|A_i|} \frac{\phi_2}{\phi(a_i)} \frac{n(t, A_i)}{N}. \end{aligned} \tag{24}$$

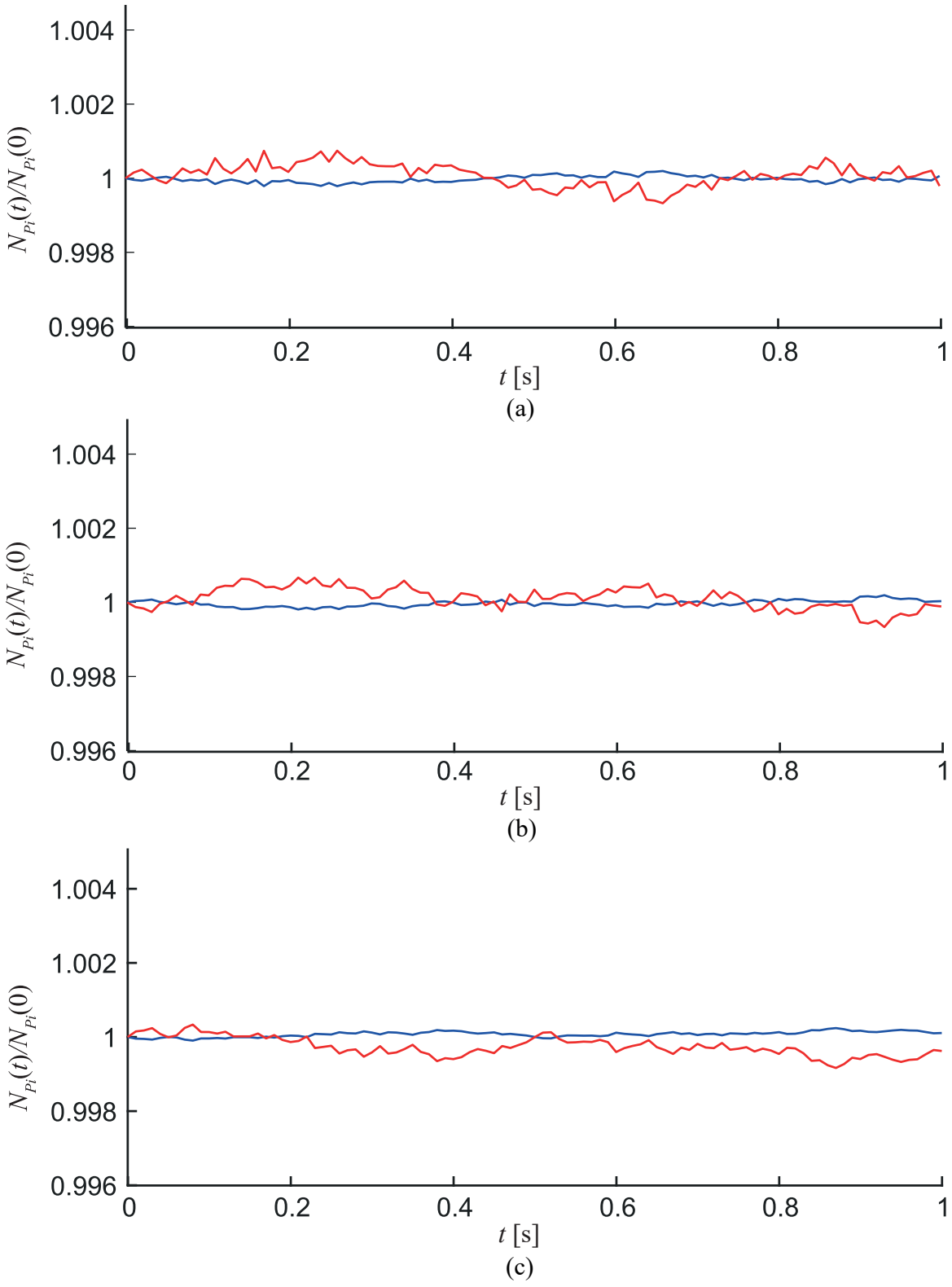

Figure 2: Case 1: Temporal variation of the ratio $n(t, R_i)/N_i$ between the number of particles at time t and $t = 0$ in R_1 (blue line) and R_2 (red line) for (a) GUM, (b) GSBM and (c) GHYMLA algorithm.

3.2.2 Numerical results

The temperature is initially assumed step-wise constant and equal to $0\,\mathrm{K}$ in R_1 and $T_0 = 283.15\,\mathrm{K}$ in R_2. The particles are initially uniformly distributed over R_2, as indicated in Figure 3. The reference temperature $T_{\mathrm{ref}}(t, a_i)$ is computed according to (23) with $y = a_i$, while the numerical temperature is defined as

$$T_{\mathrm{num}}(t, a_i) := T_0 \frac{L}{|A_i|} \frac{\phi_2}{\phi(a_i)} \frac{n(t, A_i)}{N}. \tag{25}$$

The quality of the solution is then evaluated through the root mean squared error applied to the temperature spatial distribution as different time levels

$$\mathrm{RMSE} = \sqrt{\frac{\sum_{i=1}^{N_a} (T_{\mathrm{ref}}(t, a_i) - T_{\mathrm{num}}(t, a_i))^2}{N_a}} \text{ in K}. \tag{26}$$

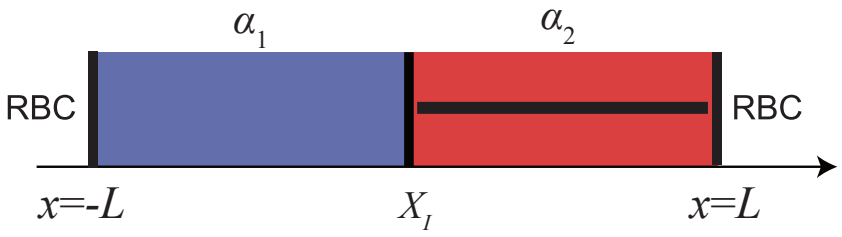

Figure 3: Case 2 setup: blue and red regions indicate R_1, R_2, the continuous black line indicates initial uniform particle placement in layer R_2.

The magnitude of the time step strongly affects accuracy. The influence of the time step on the quantification of temperature over the domain is evaluated by the RMSE between T_{ref} and T_{num} for different values of the time step Δt. As shown in Figure 4, the GSBM accuracy is essentially independent of Δt over the span of three orders of magnitudes. The GUM algorithm attains a stable value of the error for $\Delta t \leq 0.1\,\mathrm{s}$, while a sharp nonlinear increase of the error is observed for $\Delta t > 0.1\,\mathrm{s}$. This result suggests the existence of a threshold value for which we observe a correlation between RMSE and Δt for GUM, in line with [2]. However, the threshold value of Δt for which the error starts increasing is here different, suggesting that the threshold may be case-dependent.

A direct linear convergence is observed for GHYMLA, *i.e.*, the RMSE decreases linearly with Δt. For all tested values of Δt the GHYMLA algorithm is the least accurate.

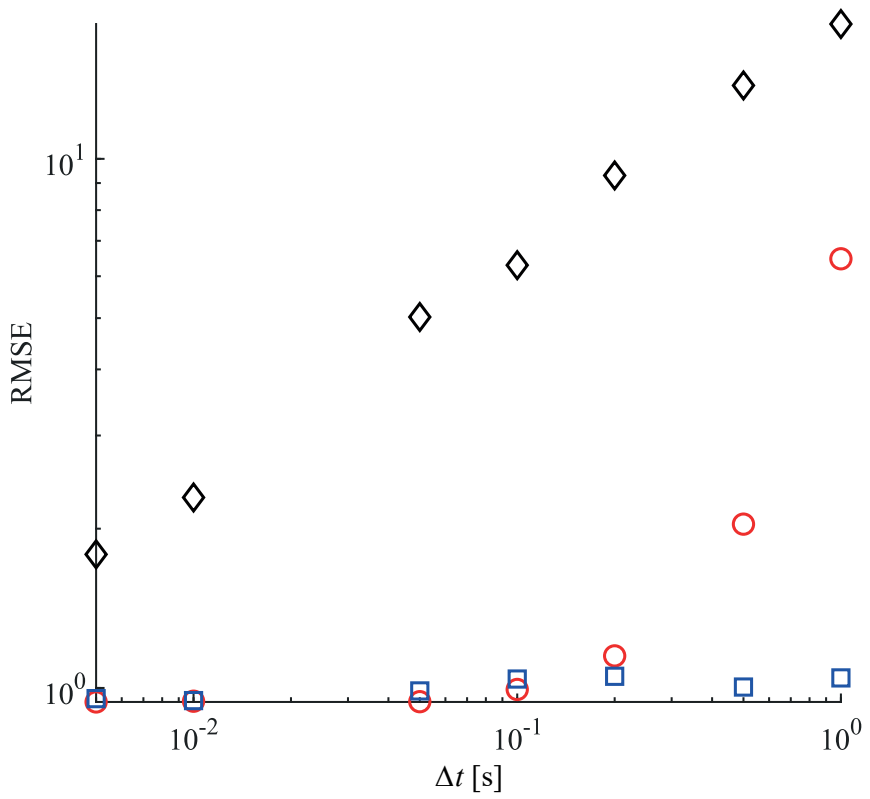

Figure 4: Case 2: RMSE between the analytical solution T_{ref} and the numerical T_{num} obtained from the GUM (red circles), GSBM (blue squares) and GHYMLA (black diamonds) for different Δt at time $t = 1\,\text{s}$.

The comparison between the analytical and the numerical temperature is displayed in Figure 5. The simulations are performed using the computational parameters in Table 3.

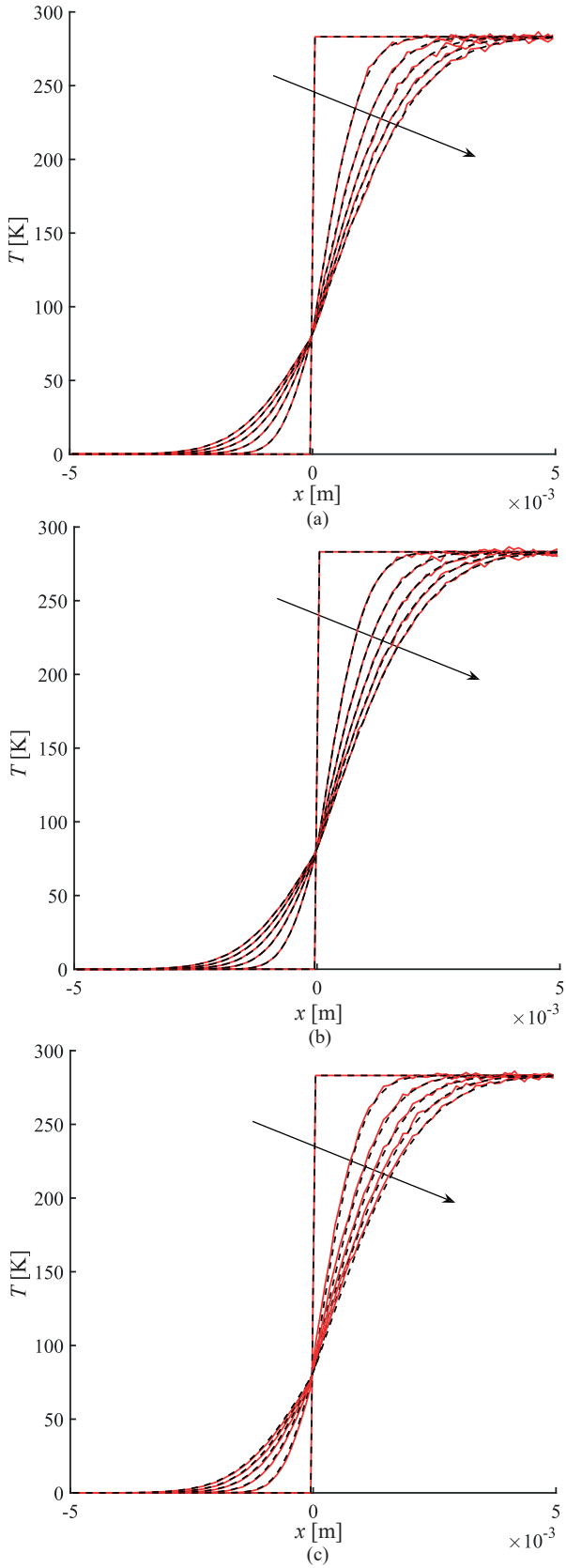

Figure 5: Case 2: Comparison between the analytical T_{ref} (black dashed line) and the numerical T_{num} (red line) temperature obtained from (a) GUM, (b) GSBM and (c) GHYMLA algorithm from the initial time to $t = 5\,\text{s}$ with a time interval of $1\,\text{s}$.

A good accuracy in simulating the analytical solution is observed for all the assessed algorithms. The RMSE between T_{ref} and T_{num} is computed for an increasing number of particles N_p as displayed in Figure 6. The GUM, GSBM, GHYMLA algorithms converge to the line $\text{RMSE} \propto N_p^{-0.5}$, *i.e.* the expected Monte Carlo convergence rate.

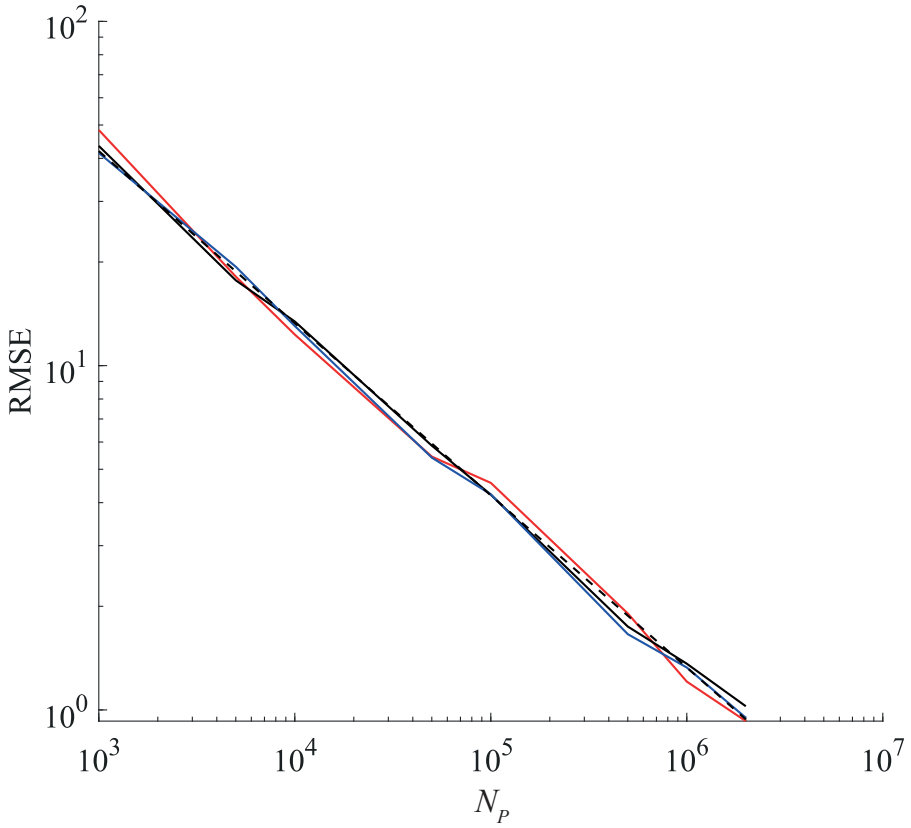

Figure 6: Case 2: RMSE between the analytical T_{ref} and the numerical T_{num} temperature obtained from GUM (red), GSBM (blue) and GHYMLA (black) for an increasing number of particles at time $t = 1\,\text{s}$. The dashed line corresponds to $\text{RMSE} \propto N_p^{-0.5}$.

Finally, we test the performance of the algorithms in estimating the temperature for different ratios between the thermal diffusivities of the two materials. The RMSE between the analytical and numerical temperature is computed for different ratio between the thermal diffusivity (α_1/α_2) in R_1 and R_2, as displayed in Figure 7. All algorithms exhibit RMSE fluctuating at a maximum of $10\,\%$ with respect to the average without showing any particular trend. The lack of a clear correlation between RMSE and α_1/α_2 indicates that the algorithms tested operate with approximately the same accuracy independent of the assumed physical parameters. As shown in Figure 7, the GSBM is on average the most accurate in estimating the temperature over the domain. For $\alpha_1/\alpha_2 = 0.25$ the three algorithms display a similar RMSE.

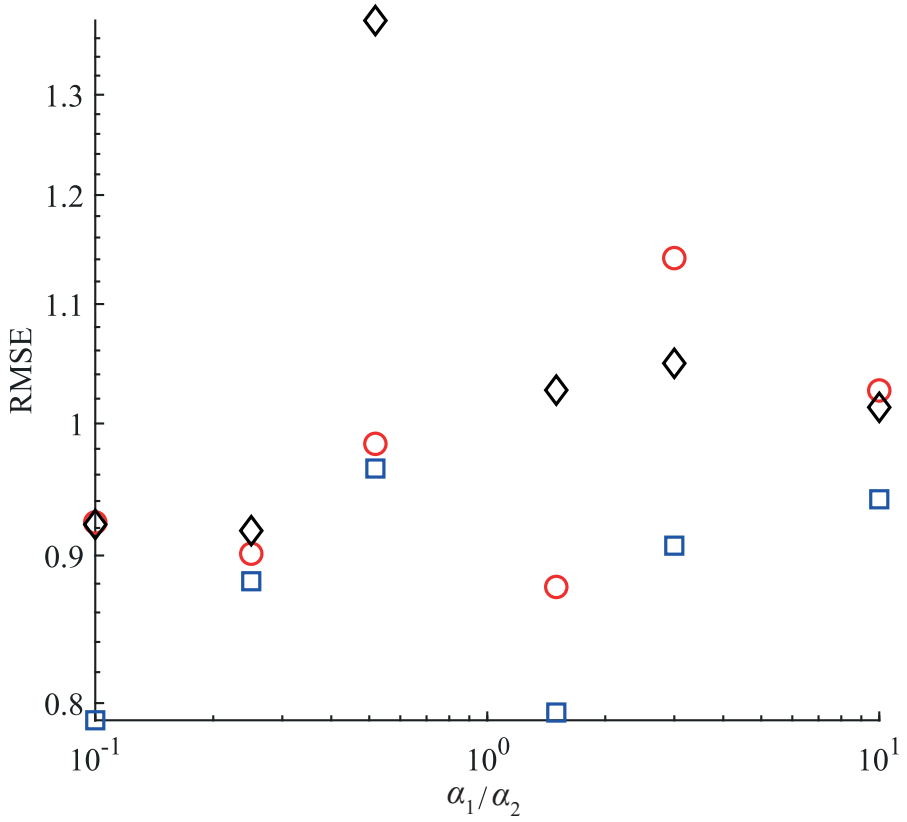

Figure 7: Case 2: Comparison of the RMSE between T_{ref} and T_{num} derived from GUM (red circles), GSBM (blue squares) and GHYMLA (black diamonds) for different α_1/α_2 values at time $t = 1\,\text{s}$. The time step Δt is assumed equal to $10^{-2}\,\text{s}$ for GSBM, $10^{-3}\,\text{s}$ for GUM and $10^{-4}\,\text{s}$ for GHYMLA.

4 Conclusions

This work applies the modeling approach presented in [2] to simulate a thermal diffusion process in discontinuous media. The GUM, GHYMLA and GSBM algorithms are here employed to assess the conductive heat transport in one-dimensional bimaterial medium. The Uffink [26] and the HYMLA [10] methods have been developed to deal with bimaterial media, with a condition that the flux is continuous (Fick's law). For other interface conditions the Uffink and HYMLA methods cannot be applied as such. It is already noted in [16] that the SBM method could deal with a wide range of conditions. Here, we show through the GSBM method how to apply it to heat transport process. Although exact, the SBM method requires the simulation of complex distributions, which hinders its computational time. Fourier's law, which is a classical formulation of the evolution of the temperature, does not allow a direct application of these methods. We introduced a new formulation using a convenient transform and shown how to implement a Lagrangian method with a weight associated to each particle.

Our work provides a critical extension of available Lagrangian methodologies to deal with heat transfer processes in the presence of material interfaces. Based on the numerical results, the following major conclusions can be drawn:

- conservation of thermal energy is verified by the GUM, GSBM and GHYMLA algorithms which are all able to maintain steady-state thermal equilibrium condition;
- the time step magnitude strongly affects the accuracy of the algorithms in estimating the temperature over the domain in GUM and GHYMLA: the GUM demonstrates sensitivity to the time step only for $\Delta t > 0.1$ s, whereas GHYMLA exhibits a direct linear correlation (in log-log) between the root-mean-square error (RMSE) and the chosen Δt. The GSBM remains independent of Δt over the span of three orders of magnitude;
- the tested algorithms demonstrate consistent accuracy regardless of the assumed physical parameters, such as thermal diffusivity contrast across the interface;
- the GUM algorithm strikes a favorable balance between accuracy and computational time, making it the preferred choice in the considered scenarios.

References

[1] A. Amiri Delouei, A. Emamian, H. Sajjadi, M. Atashafrooz, Y. Li, L.-P. Wang, D. Jing, and G. Xie. A comprehensive review on multi-dimensional heat conduction of multi-layer and composite structures: Analytical solutions. *Journal of Thermal Science*, 30(6):1875 – 1907, 2021.

[2] E. Baioni, A. Lejay, G. Pichot, and G. M. Porta. Modeling diffusion in discontinuous media under generalized discontinuous interface conditions, Part I: theory and algorithms. *Submitted to International Journal of Heat and Mass Transfer*, 2023.

[3] H. S. Carslaw and J. C. Jaeger. *Conduction of heat in solids*. Oxford University Press, 1959.

[4] W. Dahmen, T. Gotzen, S. Müller, and M. Rom. Numerical simulation of transpiration cooling through porous material. *International journal for numerical methods in fluids*, 76(6):331–365, 2014.

[5] F. de Monte. An analytic approach to the unsteady heat conduction processes in one-dimensional composite media. *International Journal of Heat and Mass Transfer*, 45(6):1333–1343, 2002.

[6] Z.-S. Deng and J. Liu. Monte Carlo method to solve multidimensional bioheat transfer problem. *Numerical Heat Transfer: Part B: Fundamentals*, 42(6):543–567, 2002.

[7] M. E Ismaeel. Heat transfer in a square porous cavity with partial heating and cooling for opposite vertical walls. *Al-Rafidain Engineering Journal (AREJ)*, 19(5):107–121, 2011.

[8] J. Fourier. *The analytical theory of heat*. New York, Dover Publishers, 1955.

[9] A. Haji-Sheikh and E. M. Sparrow. The floating random walk and its application to Monte Carlo solutions of heat equations. *SIAM Journal on Applied Mathematics*, 14(2):370–389, 1966.

[10] H. Hoteit, R. Mose, A. Younes, F. Lehmann, and P. Ackerer. Three-dimensional modeling of mass transfer in porous media using the mixed hybrid finite elements and the random-walk methods. *Mathematical Geology*, 34(4):435–456, 2002.

[11] A. J. Janavičius and S. Turskiene. Modelling of nonlinear thermodiffusion for a spherically symmetric case. *East European Journal of Physics*, 1:13–19, 2021.

[12] N. F. Jouybari, M. E. Nimvari, and W. Zhang. A comparative study of different heat transfer enhancement mechanisms in a partially porous pipe. *SN Applied Sciences*, 3:1–15, 2021.

[13] Z. A. Khan, P. A. G. Salaberri, T. M. Heenan, R. Jervis, P. R. Shearing, D. Brett, A. Elkamel, and J. T. Gostick. Probing the structure-performance relationship of lithium-ion battery cathodes using pore-networks extracted from three-phase tomograms. *Journal of The Electrochemical Society*, 167(4):040528, 2020.

[14] Z. A. Khan, T. Tranter, M. Agnaou, A. Elkamel, and J. Gostick. Dual network extraction algorithm to investigate multiple transport processes in porous materials: Image-based modeling of pore and grain scale processes. *Computers & Chemical Engineering*, 123:64–77, 2019.

[15] T. Koch, K. Weishaupt, J. Müller, B. Weigand, and R. Helmig. A (dual) network model for heat transfer in porous media: Toward efficient model concepts for coupled systems from fuel cells to heat exchangers. *Transport in Porous Media*, 140(1):107–141, 2021.

[16] A. Lejay and G. Pichot. Simulating diffusion processes in discontinuous media: a numerical scheme with constant time steps. *Journal of Computational Physics*, 231(21):7299–7314, 2012.

[17] A. Lejay and G. Pichot. Simulating diffusion processes in discontinuous media: Benchmark tests. *Journal of Computational Physics*, 314:384–413, 2016.

[18] J. Liu, P. Yu, Y. Li, C. Wan, and D. Du. Numerical simulation on convective heat transfer characteristics in porous media based on the digital rock technology. *International Journal of Heat and Mass Transfer*, 196:123323, 2022.

[19] L. Mrňa, J. Řiháček, M. Šarbort, and P. Horník. Solar absorber with a structured surface–a way to increase efficiency. *Acta Polytechnica*, 59(2):134–143, Apr. 2019.

[20] B. Noetinger, D. Roubinet, A. Russian, T. Le Borgne, F. Delay, M. Dentz, J.-R. De Dreuzy, and P. Gouze. Random walk methods for modeling hydrodynamic transport in porous and fractured media from pore to reservoir scale. *Transport in Porous Media*, 115:345–385, 2016.

[21] M. Praprotnik, M. Sterk, and R. Trobec. Inhomogeneous heat-conduction problems solved by a new explicit finite difference scheme. *International Journal of Pure and Applied Mathematics*, 13:275–292, 2004.

[22] T. Sahabi and S. Balaska. Analytical one-dimensionless study of unsteady heat transfer in bilayer, and three-layer materials. 2020.

[23] M. Sans, O. Farges, V. Schick, and G. Parent. Solving transient coupled conductive and radiative transfers in porous media with a Monte Carlo method: Characterization of thermal conductivity of foams using a numerical flash method. *International Journal of Thermal Sciences*, 179:107656, 2022.

[24] E. Shahraeeni and D. Or. Thermo-evaporative fluxes from heterogeneous porous surfaces resolved by infrared thermography. *Water resources research*, 46(9), 2010.

[25] T. Sherman, N. B. Engdahl, G. Porta, and D. Bolster. A review of spatial markov models for predicting pre-asymptotic and anomalous transport in porous and fractured media. *Journal of Contaminant Hydrology*, 236:103734, 2021.

[26] G. Uffink. Analysis of dispersion by the random walk method. *Ph.D. Dissertation, Delft University of Technology*, 1990.

[27] Y. Xu, Y. Zheng, and J. Kou. Prediction of effective thermal conductivity of porous media with fractal-Monte Carlo simulations. *Fractals*, 22(03):1440004, 2014.

[28] K. Yang, X. Li, K. Liu, and J. Wang. Coupling effect of heat transfer in plate heat exchanger filled with porous media. *International Journal of Heat and Mass Transfer*, 182:121966, 2022.